THE JOURNAL OF PHYSICAL CHEMISTRY C

Article

pubs.acs.org/JPCC

Analytical Model of CeO_2 Oxidation and Reduction

B. Bulfin,* A. J. Lowe, K. A. Keogh, B. E. Murphy, O. Lübben, S. A. Krasnikov, and I. V. Shvets

School of Physics, Trinity College Dublin, College Green, Dublin 2, Ireland

ABSTRACT: In this work, an Arrhenius-based model for the high-temperature reduction and oxidation of CeO_2 is developed. The model is shown to agree well with both literature data for the equilibrium oxygen vacancy concentration and novel experimental kinetics of oxidation and reduction obtained by the authors. The form of the Arrhenius rate equation was determined from the properties of the reaction. Equilibrium data from the literature was analyzed with respect to our rate equation. From this analysis, a number of constraints on the model parameters were determined, and some of the constants of the model were fixed. The model accurately predicts the equilibrium composition of CeO_2 over a wide range of oxygen partial pressures (10^{-2} to 10^{-8} bar) and temperatures (1000−1900 °C). Novel results of the experimental reoxidation of ceria were analyzed to fix the remainder of the constants. Porous cerium dioxide pellets produced by the authors were reduced at high temperature (1650 °C) and low oxygen partial pressure (10^{-5} bar). The reduced cerium pellets were then reoxidized in an oxygen atmosphere of 1.4×10^{-4} bar at temperatures in the range 500−1000 °C. The reoxidation was conducted in a sealed vacuum chamber. The reaction was monitored via the change in pressure and gas composition measured by a manometer and mass spectrometer. The results from this reoxidation experiment allowed us to fix the values of the activation energies and frequency factors of the oxidation and reduction. The model was then compared with experimental reaction kinetics of thermal oxidation and reduction and showed good agreement.

$$CeO_2 \underset{k_{oxidation}}{\overset{k_{reduction}}{\rightleftharpoons}} CeO_{2-\delta} + \frac{\delta}{2}O_2$$

INTRODUCTION

Cerium dioxide has found many applications due to its unique properties. At high temperatures, it is an oxide conductor and is also noted for its oxygen storage and redox properties.[1−3] This makes it a good material for applications in catalysis and solid oxide fuel cells.[4−7] Ceria has also been heavily investigated for its use in converting heat energy to fuels.[8−13] It can be thermally reduced at high temperatures, releasing oxygen.

$$CeO_2 \rightarrow CeO_{2-\delta} + \frac{\delta}{2}O_2$$

The reduced ceria can then be used to split H_2O or CO_2.[14−16]

$$CeO_{2-\delta} + \delta H_2O \rightarrow CeO_2 + \delta H_2$$

$$CeO_{2-\delta} + \delta CO_2 \rightarrow CeO_2 + \delta CO$$

Together, these products form syn-gas, which can be converted into denser diesel-type fuel using the Fischer−Tropsch process.[17] This means there are many options for fuel conversion, with the possibility of producing hydrogen, syn-gas, or diesel-type fuels. The reaction can be driven using concentrated solar power as the heat input, making these fuels renewable.[18−20] A number of reactor designs for such fuel conversion have been proposed,[21,22] and some prototypes have been constructed.[14,15,23] Alternatively, these reactions could conceivably be driven by any high-temperature heat source, making this a very attractive energy conversion technology.

In the past, studies have been conducted into developing numerical models of the phase diagrams and composition of CeO_2 over a wide range of conditions.[24−26] These models, however, give us no information about the reaction kinetics of the reduction and oxidation of ceria. It is interesting to note that ceria remains in the fluorite phase throughout the range of temperatures and pressures of interest for these fuel conversion cycles.[13,24] Even with large numbers of oxygen vacancies, the fluorite phase is still stable. The fact that no phase changes occur should allow the development of a reasonably simple model of the reactions.

The lack of such a simple analytical model for the reaction kinetics of ceria reduction makes the modeling of the performance of the above reactions difficult. If one has a simple model, which depends only on the concentrations of the reactants, the temperature, and the oxygen partial pressure, then it can easily be linked to heat flow and diffusion simulations.[27] This will greatly improve reactor design capabilities and allow for more accurate assessment of this proposed fuel production technology.

In this work, an analytical model for the reduction and oxidation of ceria in an oxygen atmosphere is developed. The model should predict both the equilibrium composition and reaction kinetics if it is to accurately simulate the performance of the reactions. It should prove to be an invaluable tool in the development of the discussed fuel production technology. It could also be of use in any cerium dioxide high-temperature redox processes. The model itself is of theoretical interest as it should allow for a better understanding of the role of diffusion and surface reactions in ceria reduction and oxidation.

Received: July 3, 2013
Revised: September 27, 2013

   dx.doi.org/10.1021/jp406578z | J. Phys. Chem. C XXXX, XXX, XXX−XXX

MODEL

The model is based on the Arrhenius equation. Because it is an equilibrium reaction, both reduction and oxidation reactions are taking place at any given time.

$$\mathrm{CeO_2} \rightleftharpoons \mathrm{CeO_{2-\delta}} + \frac{\delta}{2}\mathrm{O_2} \tag{1}$$

The reaction does not proceed to complete decomposition in this regime. If enough oxygen is removed, then the fluorite phase will no longer be stable and a phase transition will be inevitable. If there is a phase change, then the fundamental properties of the reaction kinetics will change and our equation will no longer be valid. Therefore, it is assumed that not all of the oxygen can be removed by this reaction and that it is proceeding toward a certain maximum value of δ, say x.

$$\mathrm{CeO_2} \rightarrow \mathrm{CeO_{2-x}} + \frac{x}{2}\mathrm{O_2} \tag{2}$$

The reduction reaction depends on the concentration of removable oxygen, and the oxidation reaction depends on the concentration of vacancies and the concentration of oxygen gas. Initially, oxygen diffusion in the bulk shall be ignored, and the vacancy concentration is assumed to be constant throughout. The rate of change of the oxygen vacancy concentration is the rate at which oxygen leaves CeO_2 (reduction) minus the rate at which it recombines (oxidation).

$$\frac{\mathrm{d}[\mathrm{O_{vac}}]}{\mathrm{d}t} = [\mathrm{O_{Ce}}]k_{\mathrm{red}} - [\mathrm{O_{vac}}][\mathrm{O_{gas}}]^n k_{\mathrm{ox}} \tag{3}$$

Here k_{red} and k_{ox} are the rate constants of reduction and oxidation, respectively. These rate constants take the Arrhenius form.[28]

$$k_a = A_a \exp\left(\frac{-E_a}{RT}\right) \tag{4}$$

The concentration terms can be made unitless by dividing eq 3 by the concentration of cerium [Ce], which is a constant.

$$\frac{1}{[\mathrm{Ce}]}\frac{\mathrm{d}[\mathrm{O_{vac}}]}{\mathrm{d}t} = \frac{[\mathrm{O_{Ce}}]}{[\mathrm{Ce}]}k_{\mathrm{red}} - \frac{[\mathrm{O_{vac}}]}{[\mathrm{Ce}]}[\mathrm{O_{gas}}]^n k_{\mathrm{ox}} \tag{5}$$

The rate is now in terms of moles of oxygen vacancies per mole of cerium per second or simply per second. From eqs 1 and 2, the values $[O_{Ce}]/[Ce]$ and $[O_{vac}]/[Ce]$, which are both unitless, can be defined in terms of the stoichiometry parameters δ and x.

$$\frac{[\mathrm{O_{Ce}}]}{[\mathrm{Ce}]} = x - \delta \tag{6}$$

$$\frac{[\mathrm{O_{vac}}]}{[\mathrm{Ce}]} = \delta \tag{7}$$

The oxygen gas concentration is directly proportional to the oxygen partial pressure P_{O_2}. Therefore, the constant of proportionality can simply be included as part of the rate constant k_{ox}, and the oxygen gas concentration is taken to be the oxygen partial pressure. Initially, we wish to look at equilibrium data, so we set the rate to zero. Setting eq 5 equal to zero and using eqs 4, 6, and 7, we get an equilibrium condition.

$$(x-\delta)A_{\mathrm{red}} \exp\left(\frac{-E_{\mathrm{red}}}{RT}\right) - \delta P_{\mathrm{O_2}}^n A_{\mathrm{ox}} \exp\left(\frac{-E_{\mathrm{ox}}}{RT}\right) = 0 \tag{8}$$

At equilibrium, the rate of oxidation is equal to the rate of reduction. We can now express our equilibrium oxygen vacancy concentration as a function of temperature and oxygen partial pressure.

$$\left(\frac{\delta}{x-\delta}\right) = \frac{A_{\mathrm{red}}}{A_{\mathrm{ox}}} P_{\mathrm{O_2}}^{-n} \exp\left(\frac{-(E_{\mathrm{red}} - E_{\mathrm{ox}})}{RT}\right) \tag{9}$$

The difference in activation energies $E_{red} - E_{ox}$ shall be labeled throughout the remainder of the manuscript as ΔE.

Equilibrium Composition. It is common in the literature for equilibrium data obtained at constant temperature and varied pressure to plot $\log(\delta)$ versus $\log(P_{O_2})$. If the logarithm of eq 9 is taken, it is clear that a more suitable plot can be made.

$$\log\left(\frac{\delta}{x-\delta}\right) = -n\log(P_{\mathrm{O_2}}) + \log\left(\frac{A_{\mathrm{red}}}{A_{\mathrm{ox}}}\exp\left(\frac{-\Delta E}{RT}\right)\right) \tag{10}$$

From eq 10, it is clear that a plot of $\log(\delta)$ versus $\log(P_{O_2})$ will yield a straight line with slope $-n$ but only when $\delta \ll x$. Supporting this, both Panlener and Dawicke[29,30] found that in the region $0.001 < \delta < 0.004$ this plot yields a straight line, and the pressure dependence was well-characterized by the relation $\delta \propto P_{O_2}^{-1/5}$.

Because we are not dealing with a dilute species reaction, it may not be possible to use the law of mass action to accurately find x and n. It can, however, provide a good starting point. From eq 2, the law of mass action predicts that $n = x/2$. Using the findings of Panlener et al., as an estimate of $n = 0.2$, a good starting point would be to set $x = 0.4$. Using these parameters, experimental equilibrium data can be analyzed. Data in the range 1000−1500 °C were extracted from the experimental work of Panlener et al.[29] For temperatures above this, the numerical model of Zinkevich et al.[24] was used, which is in good agreement with experimental findings.[29−33] We look at pressures in the range of 10^{-2} to 10^{-9} bar.

The analysis of data from the literature is presented in Figure 1, with the parameter $x = 0.35$. For constant temperature, the data show linear dependencies over a wide range of pressures. This is in contrast with the plots made previously of $\log(\delta)$ versus $\log(P_{O_2})$,[29] where the data begin to deviate from the linear dependence as δ increases and drastically so for values of δ greater than 0.1. This is as predicted by eq 8, providing strong evidence in support of our analytical model.

To determine the best value of x, we plotted the data for a range of different values of x. The plots were then fit linearly, and the variation in slope and the R^2 regression value of each set of data was compared.

The dependency of slope on the temperature is plotted in Figure 2. For simplicity, we want the value of n to be constant. The best choice of x would therefore be that which gives the least variation in slope. Comparing the statistics of the range of slopes obtained for each value of x, the value of x that gives the lowest standard deviation is $x = 0.35$. Taking the average of these slopes to be n and the standard deviation to be the error, we get $n = 0.218 \pm 0.013$.

To evaluate each linear fit, the variance in the R^2 regression value was plotted against temperature. From Figure 3, we can see that for $x = 0.33$ the R^2 regression value drops below 0.96 at

dx.doi.org/10.1021/jp406578z | J. Phys. Chem. C XXXX, XXX, XXX−XXX

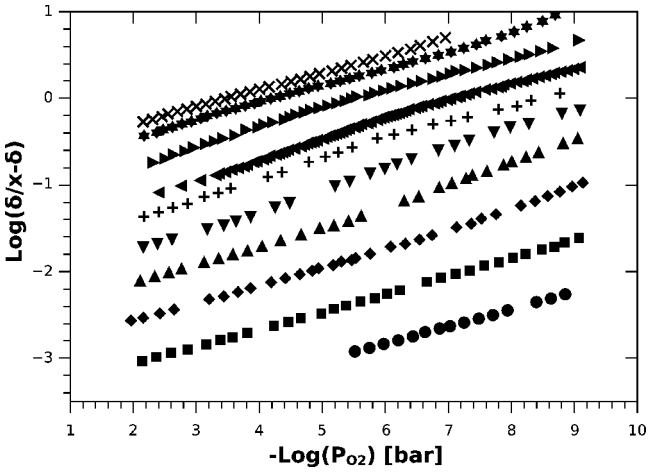

Figure 1. Isothermal plots of $\log(\delta/(x-\delta))$ versus $-\log(P_{O_2})$ with the value of x set to 0.35. The temperatures plotted are from bottom to top 1000, 1100, 1200, 1300, 1400, 1500, 1587, 1725,1850, and 1930 °C. The data are taken from Panlener et al.[29] and Zinkevich et al.[24]

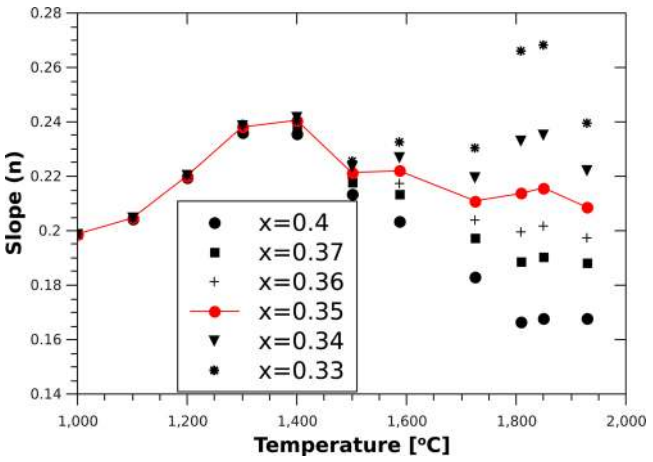

Figure 2. Slope obtained from a linear fit of $\log(\delta/(x-\delta))$ versus $-\log(P_{O_2})$ plotted against temperature for six different values of the parameter x.

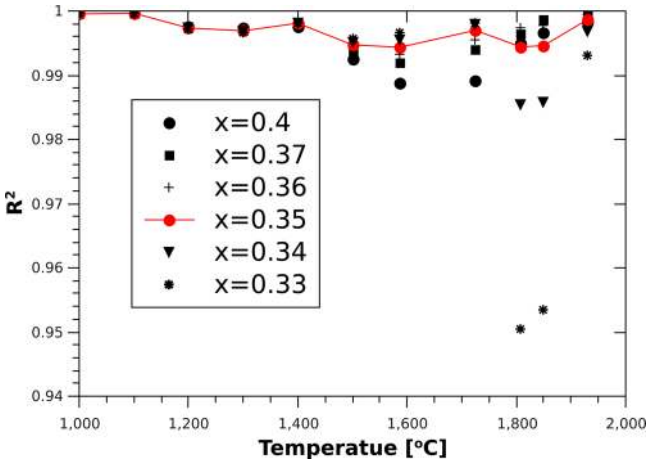

Figure 3. R^2 value obtained from a linear fit of $\log(\delta/(x-\delta))$ versus $-\log(P_{O_2})$ plotted against temperature for five different values of the parameter x.

high temperatures. The rest of the values of x give good linear fits over the range investigated, with x = 0.35 to 0.36 having the best average values, both around R^2 = 0.997. The value x = 0.35 gave the most consistent slope and is the best fit of the published equilibrium data.

The best fit value of x = 0.35 can now be applied to further analyze the equilibrium data. Taking the natural logarithm of eq 9 allows us to easily extract the difference in activation energies ΔE.

$$\ln\left(\frac{\delta}{x-\delta}\right) = \frac{-\Delta E}{RT} + \ln\left(P_{O_2}^{n}\frac{A_{red}}{A_{ox}}\right) \quad (11)$$

Each set of data plotted in Figure 4 was fit linearly. Taking the average value calculated from the slopes as the activation energy and the standard deviation as the error, we get ΔE = 195.6 ± 1.2 kJ mol^{-1}.

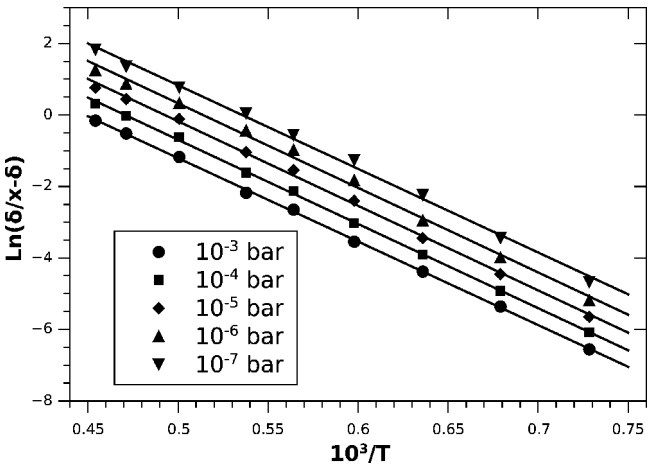

Figure 4. A graph of $\ln(\delta/(x-\delta))$ versus $10^3/T$ for a range of different pressures. The data are again taken from Panlener et al.[29] and Zinkevich et al.[24] The data were fit linearly, and from the slope of each line we can calculate the difference in activation energies ΔE.

We can now use our values of x, n, and E to get information from the intercepts of Figures 1 and 4. This will allow us to determine the ratio between the frequency factors A_{red}/A_{ox}. Taking the average of all of the values determined from the linear fit intercepts of Figures 1 and 4 and taking the standard deviation as the error, we get A_{red}/A_{ox} = 8700 ± 800 bar^n. The units of bar^n are from our choice to absorb the constant of proportionality between the oxygen partial pressure and the oxygen gas concentration into A_{ox}.

$$\left(\frac{\delta}{0.35-\delta}\right) = 8700 \times P_{O_2}^{-0.217}\exp\left(\frac{-195.6\ \text{kJ mol}^{-1}}{RT}\right) \quad (12)$$

Substituting the above values into eq 9 yields eq 12, which depends only on the oxygen partial pressure and temperature. In Figure 5, we plot the results of the fits along with the original data from Figure 4 on a linear scale. As can be seen, the results of the fit match the original data quite well on a linear scale.

Reaction Kinetics. For oxygen to leave CeO_2, it must first diffuse to the surface. This diffusion process may conversely be considered as the diffusion of oxygen vacancies. For simplicity, we will consider spherical particles. This means we can use the

dx.doi.org/10.1021/jp406578z | J. Phys. Chem. C XXXX, XXX, XXX−XXX

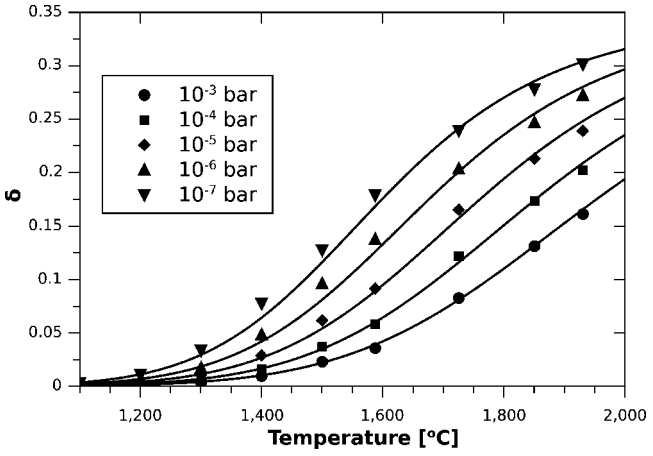

Figure 5. Plot of the vacancy concentration δ versus temperature. The points are the same as Figure 4, plotted with the results of fitting the analytical model to the same data.

spherically symmetric diffusion equation, where the solution depends only on the radial position.

$$\frac{\partial C(T, t, r)}{\partial t} = \frac{1}{r^2}\frac{\partial}{\partial r}D(C, T)r^2\frac{\partial C(T, t, r)}{\partial r} \quad (13)$$

The boundary condition at the surface of a spherical particle of radius R can now be set as our reaction rate formula shown in eqs 5 and 8. As before, the units could be simplified by dividing each concentration by the concentration of cerium.

$$\frac{\partial C_R}{\partial t} = (C_m - C_R)A_{red}\exp\left(\frac{-E_{red}}{RT}\right) - C_R P_{O_2}^n A_{ox}\exp\left(\frac{-E_{ox}}{RT}\right) \quad (14)$$

If we know our diffusion coefficient, D, and our particle radius, R, the problem is a simple partial differential equation in one spatial dimension. The diffusion coefficient for CeO_2 can generally be well-described with an Arrhenius dependence on temperature.[34,35]

$$D(T) = D_o\exp\left(\frac{-E_d}{RT}\right) \quad (15)$$

As we deviate from stoichiometry and the concentration of oxygen vacancies increases, the diffusion coefficient will also increase. Therefore, our complete diffusion coefficient is a function of both temperature and oxygen vacancy concentration.[36]

$$D(C, T) = D_o(C)\exp\left(\frac{-E_d(C)}{RT}\right) \quad (16)$$

In the temperature range 900−1100 °C and for vacancy concentrations δ in the range 0 to 0.2, Stan et al.[37] found that both $D_o(C)$ and the diffusion activation energy $E_d(C)$ were well-described by a linear dependence on C. The temperature range, however, is too narrow for use in this work. Here we are dealing with a wide range of temperatures and oxygen partial pressures, and so a full analytical solution of the diffusion problem is impractical. We will later simplify the effect of diffusion by assuming a shrinking core model.

To complete the rate equation, the values of E_{red} and A_{red} or E_{ox} and A_{ox} need to be determined. During the reduction of ceria at high temperature, the kinetics are determined by the balance between both the oxidation and reduction terms in our equation. There are sources that suggest activation energies for the reduction reaction,[38−40] although the values vary from 101.2[39] to 221 kJ mol^{-1}.[38] It is also difficult to determine exactly what activation energy they have extracted from the data due to the combination of oxidation and reduction.

Instead, consider the oxidation of oxygen-deficient ceria at moderate temperatures. At relatively moderate temperatures (500−1000 °C), the reduction term should be very small relative to the oxidation term due to its much larger activation energy ($E_{red} - E_{ox} \approx 196$ kJ mol^{-1}). So, at moderate temperatures, we can treat the reaction kinetics for a reduced sample as only the oxidation term in eq 5, resulting in eq 17.

$$\frac{d\delta}{dt} = -\delta P_{O_2}^n A_{ox}\exp\left(\frac{-E_{ox}}{RT}\right) \quad (17)$$

By examining this reaction, it should be possible to determine the remainder of the unknown constants in the rate equation.

EXPERIMENTAL PROCEDURE

In our experiments, we aim to investigate both the backward and forward reactions of the equilibrium reaction shown in eq 1. In other words, when displaced from equilibrium in either direction, how quickly does the system return to equilibrium? Most importantly, we first wish to investigate the reoxidation of cerium because, according to eq 17, this should allow us to extract E_{ox} and A_{ox}.

An apparatus was built by the authors, which allows oxides to be heated to high temperatures in a controlled atmosphere. The apparatus consists of a vacuum chamber in which the sample is placed and a focused Xenon lamp for rapidly heating the sample to reaction temperatures. The Xenon lamp uses an elliptical mirror to focus 100 W of broadband power into a focal point <8 mm in diameter. This allows temperatures up to 1650 °C to be achieved.

Changes in pressure are measured using a capacitance manometer, and the gas composition is monitored using a mass spectrometer. Oxygen released from the sample is observed by an increase in pressure and an increase in the oxygen signal measured by the mass spectrometer. Conversely, oxygen absorbed by the sample is accompanied by a drop in pressure and a drop in the oxygen signal.

Figure 6 shows a schematic of our apparatus. The type-B thermocouple is placed on top of the sample, and the Xenon lamp is focused onto the sample and thermocouple. The sample holder is an alumina crucible surrounded by another layer of alumina to protect the steel chamber from the high temperatures.

A reduction cycle is started by pumping the chamber down to 10^{-5} bar and then sealing the chamber off from the pump. The lamp is then switched on to heat the sample to high temperatures. The changes in sample temperature, gas temperature, pressure, and gas composition are recorded.

A reoxidation cycle is conducted by first pumping the chamber down to 10^{-5} bar; the chamber is then backfilled with oxygen to a pressure of $P_{O_2} = 1.4 \times 10^{-4}$ bar. This pressure was selected to give us a measurable reaction rate at the temperatures used for reoxidation (500−1000°C). The sample is then heated using the Xenon lamp with the input power

dx.doi.org/10.1021/jp406578z | J. Phys. Chem. C XXXX, XXX, XXX−XXX

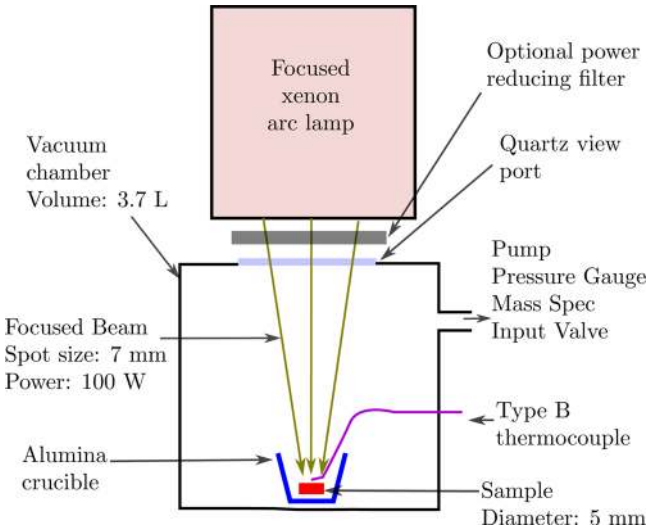

Figure 6. Apparatus showing the vacuum chamber, Xenon lamp, sample, thermocouple, and connected instruments.

reduced by a filter. The changes in temperature, pressure, and gas composition are again recorded.

The background pressure increase due to heating of the chamber without a sample present was taken into account. In the case of the reoxidation cycles, the power incident into the chamber is relatively moderate and the increase in pressure is negligible.

One issue identified with the system is that for the high-temperature reduction cycles the oxygen given off was seen to take part in other reactions as the cycle proceeds. This was observed as a decrease in the oxygen signal from the mass spectrometer and an increase in the carbon dioxide signal. No such competing reactions were observed in the reoxidation cycles. We believe that the high power incident into our chamber during the reduction cycles is causing reactions with the chamber walls. For this reason, our system is less accurate in measuring reduction than oxidation. This is not a big problem because the main experimental focus is on reoxidation, and reduction experiments will be used only for comparison with the model.

The samples used are porous pellets of CeO_2. They were prepared by mixing CeO_2 powder (Sigma-Aldrich: 544841) with a grain size <25 nm and graphite powder (Sigma-Aldrich: 282863) with a grain size <20 μm. They were mixed in a volumetric ratio of three parts graphite to one part ceria. The powders were thoroughly mixed by placing them in a beaker and vibrating them in a sonic bath for 15 min. Additionally, polished ball bearings were placed in the beaker to accelerate mixing. The mixed powder was then pressed into pellets using a pellet die and a hydraulic press. The pellets are then annealed at 1000 °C for 3 h to remove the graphite. This was followed by 24 h of annealing at 1500 °C to induce sintering. The sintered pellets are on average 4.5 mm in diameter and 1 mm in height. The porosity was calculated by measuring the mass and volume of the samples to be in the range 60−65% void space, and their masses were in the range of 28−30 mg (Figure 7).

The arc lamp focuses the light into a spot ∼7 mm in diameter; therefore, the entire sample fits into the focal point. For this reason, we believe that the temperature gradients throughout the sample will be small, and in the analysis, it is assumed that the sample temperature was uniform.

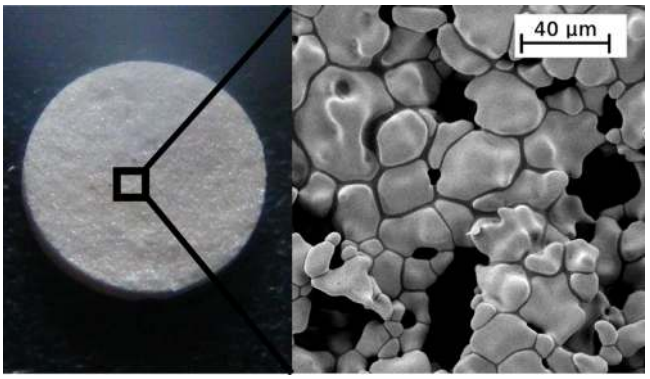

Figure 7. Image of a sample with an image taken using a scanning electron microscope showing its porosity.

EXPERIMENTAL RESULTS

As previously described, we will first look at the reoxidation of reduced cerium to determine our constants for eq 16.

$$CeO_{2-\delta} \rightarrow CeO_{2-\delta} + \frac{\delta}{2}O_2 \quad (18)$$

Typically in these oxidation experiments, the total amount of oxygen absorbed was in the range of δ = 0.06 to 0.07. Again here, δ is a dimensionless number of moles of vacancies per moles of cerium. The variance was thought to come from the reduction step carried out prior to the start of the experiment, and the samples were assumed to be fully reoxidized at the end of the experiment. This is an approximation, as there will still be a number of vacancies present because the reaction has reached equilibrium; however, the concentration of vacancies can be assumed to be small.

The volume of the chamber, changes in pressure, and gas temperature are all known. Therefore, using the formula $\Delta PV = \Delta nRT$, the number of moles of oxygen that have been absorbed by the sample can be calculated. For the initial phase of the reaction, the rate-determining feature is the reaction at the surface and not the diffusion through the bulk. Additionally, to make an Arrhenius plot, a varying temperature is needed that happens during the initial stage of the reaction. For this, it is convenient to study the reaction in the region of 0−40% completion, before the temperature starts leveling off. Equation 17 can be rearranged to get a suitable plot for extracting the activation energy E_{ox} and frequency factor A_{ox}.

$$\ln\left(-\frac{d\delta}{dt}\right) - \ln(\delta P_{O_2}^n) = \frac{-E_{ox}}{RT} + \ln(A_{ox}) \quad (19)$$

This can be thought of as an Arrhenius plot of $\ln(k)$ versus $10^3/T$. The values of δ and P_{O_2} are calculated from the data obtained from the pressure manometer and mass spectrometer. A number of cycles were conducted. All cycles started at room temperature similar to that shown in Figure 8. The cycles were run for a range of different input powers, with the final temperatures reached in the range 500−1000 °C. We assume that in this range the reaction kinetics are still of the type discussed and should be well-described by eq 19.

The data were analyzed with a regression fit as seen in Figure 9, and the 95% confidence interval was taken as the error in the slope and the intercept. The oxidation activation energy was calculated to be E_{ox}= 36 ± 4 kJ mol^{-1}, and the intercept was found to be $\ln(A_{ox})$ = 4.4 ± 0.5. This intercept value gives the frequency factor A_{ox} = 82 ± 41 s^{-1} bar^{-n}. This value should

dx.doi.org/10.1021/jp406578z | J. Phys. Chem. C XXXX, XXX, XXX−XXX

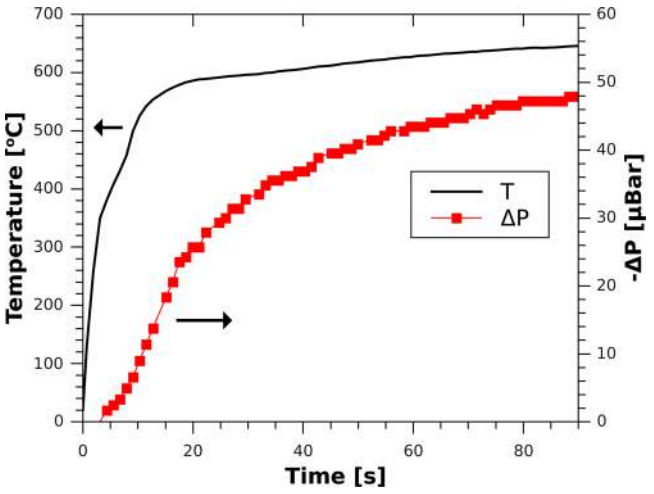

Figure 8. Graph showing sample temperature and the drop in pressure for the reoxidation of a Ceria pellet.

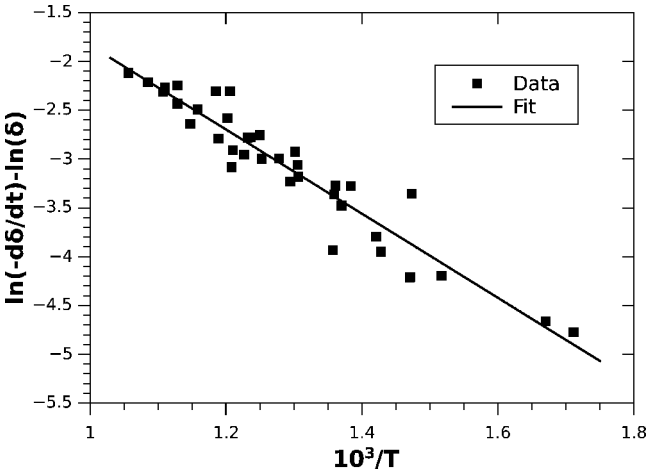

Figure 9. Plot of $\ln(k)$ versus $10^3/T$. These points are from several different scans with the final temperatures reached in the range 500–1000 °C.

depend on the surface to volume ratio. The value of surface-to-volume ratio will change due to sintering during the reduction, so the low precision for the value A_{ox} is not surprising. However, the ratio between the frequency factors A_{red}/A_{ox} is a characteristic property of the material and was determined with greater precision.

E_{red} and A_{red} can now be calculated using our values for E_{ox}, A_{ox}, and the results from the analysis of equilibrium data for ΔE and A_{red}/A_{ox}. In summary, we have the following equation with the values given in Table 1.

$$\frac{d\delta}{dt} = (x - \delta)A_{red}\exp\left(\frac{-E_{red}}{RT}\right) - \delta P_{O_2}^{n} A_{ox}\exp\left(\frac{-E_{ox}}{RT}\right) \quad (20)$$

The oxygen partial pressure is in bar; if another unit is used, the value of A_{ox} must be changed accordingly. Remember, the rate equation has been divided by the concentration of cerium to make the concentration terms unitless. Therefore, this rate must be multiplied by the concentration of cerium to get the absolute rate of reaction. The oxidation term in the ranges of temperature, oxygen partial pressure, and vacancy concentration considered in our reoxidation experiment can now be calculated to be at least four orders of magnitude greater than the reduction term in our rate equation.

Table 1. Constants in Equation 20

x	0.35
n	0.218 ± 0.0013
ΔE	195.6 ± 1.2 kJ mol^{-1}
E_{red}	232 ± 5 kJ mol^{-1}
E_{ox}	36 ± 4 kJ mol^{-1}
A_{red}/A_{ox}	8700 ± 800 bar^n
A_{red}	720 000 ± 360 000 s^{-1}
A_{ox}	82 ± 41 s^{-1} bar^{-n}

Model versus Experiment. To test the model, we can compare our reoxidation reactions to ones predicted by the model. The temperatures recorded by the thermocouple were used in a numerical model of the rate. The oxygen partial pressure is set to be the same as the initial value and is reduced proportionally as the reaction proceeds. To account for diffusion in the later stages of the reaction, a shrinking particle model is used. In particular, the case of a small particle in which the surface reaction is the rate-determining step is employed.[41] This assumes that there is a shrinking sphere of vacancies and introduces a restriction on our rate as we proceed.

$$\frac{d\delta}{dt} = \text{rate} \times (1 - \alpha)^{1/3} \quad (21)$$

where rate in eq 21 corresponds to the rate given in eq 20. The fraction-completed α is the amount of absorbed oxygen divided by the total final absorbed oxygen. This is a simplification of the effect of diffusion; for a full analytical solution, one must solve eqs 13 and 14 on a suitable sized sphere. It is assumed that the reoxidation proceeds to the final fully oxidized state with $\delta = 0$.

From Figure 10, it can be seen that the experimental results agree well with the model. If the diffusion term is omitted after the initial stages of the reaction, then the model predicts faster oxidation than was experimentally observed.

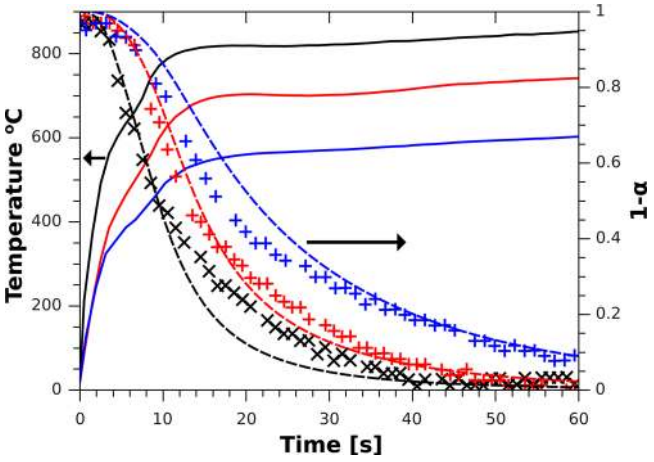

Figure 10. Experimental temperature and the corresponding fraction of remaining oxygen vacancies for three different input powers. The solid lines are the temperature, the crosses are the experimental fraction of remaining oxygen vacancies, and the dashed lines are those predicted by eq 21

The rate of the reduction reaction of CeO_2 can also be compared with the model. Again, eq 21 is used to model the reaction. In the experiment, the parameters are measured once

dx.doi.org/10.1021/jp406578z | J. Phys. Chem. C XXXX, XXX, XXX–XXX

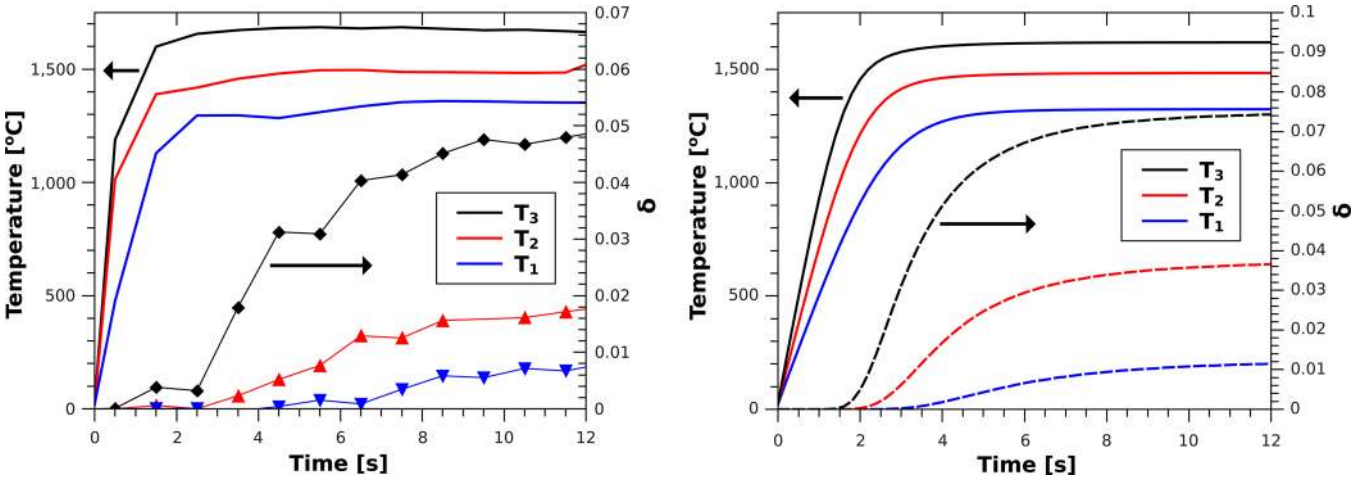

Figure 11. Left: Experimental temperature and the corresponding measured δ for three different input powers. Right: A numerical model with similar temperature curves and the corresponding numerical rates predicted.

every second; however, the reduction reaction proceeds very rapidly, and so our temperature curves have low resolution. For this reason, analytical curves of radiative heating, which are very similar to the ones seen in the experiment, were used in the numerical model. In this case, the value α is more difficult to determine. As the temperature and oxygen pressure change, so does the equilibrium δ (Figure11). The fraction-completed α can be defined as the instantaneous value of δ divided by the equilibrium value, so to determine α, we must recalculate both the equilibrium δ and the actual δ in each iteration of the numerical model. Again, as the reaction proceeds, the oxygen partial pressure in the model increases accordingly, just as it would in the experiment.

The rate curves observed in the experiment have very similar shapes to those predicted by our model. The model predicts a somewhat faster reaction, which could be attributed to the assumption that the entire pellet is uniformly heated. In reality, the bottom of the pellet is heated at a lower rate as the pellet is a porous ceramic, which has poor heat-transfer properties.[27] This will reduce the rate. The final value in the model is that of equilibrium, but in our experiment the final values were all roughly 30% lower than predicted by the model. This could be due to reactions with the chamber walls absorbing oxygen, as described in the experimental procedure. It could also be due to trapped unreacted oxide in our pellets.

DISCUSSION

The discussed model of the kinetics of the high-temperature reduction and oxidation of cerium dioxide agrees well with the equilibrium and kinetic data presented in this work; however, the model kinetics remain to be tested over a wider range of temperatures and pressures.

Theoretical Issues. It should be noted that the activation energy for reduction found here of $E_{red} = 232 \pm 5$ kJmol^{-1} is far lower than the overall change in enthalpy $\Delta H \approx 480$ kJmol^{-1} for ceria reduction.[29] However, it is widely believed that producing an oxygen vacancy at the surface of ceria takes less energy than creating a vacancy in the bulk. The change in enthalpy is then broken up into two parts, the energy change required to produce a vacancy at the surface plus the energy change due to migration of this vacancy to the bulk. In the review by Sauer et al.,[42] a value of 321 kJ mol^{-1} is given in table 4 for oxygen vacancy formation at the surface.

These formation energies are still a good deal larger than the activation energy we have found. However, this formation of a surface vacancy could itself be a multi-step process. For example, initially an oxygen surface defect could be formed in which an oxygen molecule is displaced from its usual position; this oxygen molecule could then be removed from the surface more easily. Either of these steps could then be the rate-determining step. The activation energy required to produce a vacancy could then be as low as the value we have found. This low activation energy may also explain the relative ease at which oxygen vacancies can be formed in ceria despite the large enthalpy of formation for bulk vacancies.

The activation energies determined experimentally by other authors for the thermal reduction of cerium are also very low when compared with the enthalpy of formation. A value of 221 kJmol^{-1} was obtained by Le Gal and Abanades for the reduction of cerium dioxide doped with zirconium.[38] This is lower than the value found here for pure cerium dioxide, which makes sense, as a higher oxygen yield is obtained when cerium is doped with zirconium, which would imply a lower activation energy. In the work presented by Ramos-Fernandez at The Materials for Energy conference held in Karslruhe Germany, they found an activation energy for the reduction of pure ceria to be 236 kJ mol^{-1},[43] which is within the error of the value found in this work.

Different surfaces of ceria will also have different formation energies for oxygen vacancies. This should not affect the bulk thermodynamics but may have an effect on the kinetics. We cannot bring further clarity to this issue as our experiments were carried out with polycrystalline samples. Our values for activation energies are representative of averages over the various facets present in the ceria pellets.

Model Applications. This model should be particularly useful in the development and assessment of syn-gas producing reactors based on the ceria redox system. It can easily be coupled to heat flow simulations; one simply needs to introduce a heat source to account for the reaction consuming or producing heat.

$$Q = \frac{d\delta}{dt}\Delta H \quad (22)$$

Here the heat produced is the rate times the change in enthalpy for the reaction, which is known.[29]

dx.doi.org/10.1021/jp406578z | J. Phys. Chem. C XXXX, XXX, XXX−XXX

In the case where dopants are added to ceria to improve the stability and reaction yields, we should be able to modify our equation to suit. Both ZrO_2 and HfO_2 have been shown to improve the high-temperature redox properties of CeO_2.[9,44−46] The crystal structure, however, remains unchanged, and so the same reaction model should still be applicable with a suitable change in the constants.

The model also gives us the boundary condition for the diffusion equation if the ceria is in an oxygen atmosphere. This should allow for a more in depth study of the effect of temperature and composition on the diffusion of oxygen in the bulk.

CONCLUSIONS

An Arrhenius-type model for the thermal reduction and oxidation of CeO_2 in an oxygen atmosphere was developed. The model was developed by considering the processes involved in the reactions. By analyzing equilibrium data from the literature with our model as a template, we were able to fix the difference between the activation energies of reduction and oxidation, the oxygen partial pressure dependence, the ratio of the frequency factors, and the maximum removable oxygen in this reaction regime. The resulting analytical model of the equilibrium composition is seen in eq 12. We then examined the reoxidation of cerium to determine the activation energy and frequency factor for the reoxidation term in the model. This fixed the remainder of the constants involved in the model, which are all listed in Table 1. The model's reaction kinetics were then compared with novel experimental data. The experimental results agree well with the model predictions in the temperature and pressure ranges examined.

AUTHOR INFORMATION

Corresponding Author

*E-mail: bulfinb@tcd.ie.

Notes

The authors declare no competing financial interest.

ACKNOWLEDGMENTS

This work has received funding from SFI-12/IA/1264, and the International Graduate Research Programme in Micro- & Nano Engineering, an IRCSET graduate research education programme. It was conducted in association with the Cleaner Energy Lab Trinity College Dublin.

NOMENCLATURE

δ, oxygen stoichiometry; x, maximum δ; $[O_{Ce}]$, removable oxygen concentration; $[O_{vac}]$, oxygen vacancy concentration; $[O_{gas}]$, oxygen gas concentration; $[Ce]$, concentration of cerium; n, oxygen gas power dependency; k_a, rate constant; A_a, frequency factor; E_{red}, activation energy for reduction; E_{ox}, activation energy for oxidation; P_{O_2}, oxygen partial pressure; D, diffusion coefficient; C, local vacancy concentration; C_R, boundary vacancy concentration; C_m, maximum C_R; α, fraction completed; ΔH, change in enthalpy

REFERENCES

(1) Trovarelli, A. *Comments Inorg. Chem.* **1999**, *20*, 263−284.
(2) Imagawa, H.; Suda, A.; Yamamura, K.; Sun, S. *J. Phys. Chem. C* **2011**, *115*, 1740−1745.
(3) Subbarao, E.; Maiti, H. *Solid State Ionics* **1984**, *11*, 317−338.
(4) Wilson, E. L.; Grau-Crespo, R.; Pang, C. L.; Cabailh, G.; Chen, Q.; Purton, J. A.; Catlow, C. R. A.; Brown, W. A.; de Leeuw, N. H.; Thornton, G. *J. Phys. Chem. C* **2008**, *112*, 10918−10922.
(5) Nolan, M.; Parker, S. C.; Watson, G. W. *J. Phys. Chem. B* **2006**, *110*, 2256−2262.
(6) Kharton, V.; Figueiredo, F.; Navarro, L.; Naumovich, E.; Kovalevsky, A.; Yaremchenko, A.; Viskup, A.; Carneiro, A.; Marques, F.; Frade, J. *J. Mater. Sci.* **2001**, *36*, 1105−1117.
(7) Stambouli, A.; Traversa, E. *Renewable Sustainable Energy Rev.* **2002**, *6*, 433−455.
(8) Le Gal, A.; Abanades, S.; Flamant, G. *Energy Fuels* **2011**, *25*, 4836−4845.
(9) Le Gal, A.; Abanades, S. *J. Phys. Chem. C* **2012**, *116*, 13516−13523.
(10) Kaneko, H.; Ishihara, H.; Taku, S.; Naganuma, Y.; Hasegawa, N.; Tamaura, Y. *J. Mater. Sci.* **2008**, *43*, 3153−3161.
(11) Kodama, T.; Gokon, N. *Chem. Rev.* **2007**, *107*, 4048−4077.
(12) Gokon, N.; Kodama, T.; Imaizumi, N.; Umeda, J.; Seo, T. *Int. J. Hydrogen Energy* **2011**, *36*, 2014−2028.
(13) Chueh, W. C.; Haile, S. M. *Philos. Trans. R. Soc., A* **2010**, *368*, 3269−3294.
(14) Furler, P.; Scheffe, J. R.; Steinfeld, A. *Energy Environ. Sci.* **2012**, *5*, 6098−6103.
(15) Chueh, W. C.; Falter, C.; Abbott, M.; Scipio, D.; Furler, P.; Haile, S. M.; Steinfeld, A. *Science* **2010**, *330*, 1797−1801.
(16) Rudisill, S. G.; Venstrom, L. J.; Petkovich, N. D.; Quan, T.; Hein, N.; Boman, D. B.; Davidson, J. H.; Stein, A. *J. Phys. Chem. C* **2013**, *117*, 1692−1700.
(17) Dry, M. E. *J. Chem. Technol. Biotechnol.* **2002**, *77*, 43−50.
(18) Kodama, T. *Prog. Energy Combust. Sci.* **2003**, *29*, 567−597.
(19) Steinfeld, A. *Sol. Energy* **2005**, *78*, 603−615.
(20) Abanades, S.; Charvin, P.; Flamant, G.; Neveu, P. *Energy* **2006**, *31*, 2805−2822.
(21) Villafn-Vidales, H.; Arancibia-Bulnes, C.; Dehesa-Carrasco, U.; Romero-Paredes, H. *Int. J. Hydrogen Energy* **2009**, *34*, 115−124.
(22) Miller, J.; Allendorf, M.; Diver, R.; Evans, L.; Siegel, N.; Stuecker, J. *J. Mater. Sci.* **2008**, *43*, 4714−4728.
(23) Kaneko, H.; Miura, T.; Fuse, A.; Ishihara, H.; Taku, S.; Fukuzumi, H.; Naganuma, Y.; Tamaura, Y. *Energy Fuels* **2007**, *21*, 2287−2293.
(24) Zinkevich, M.; Djurovic, D.; Aldinger, F. *Solid State Ionics* **2006**, *177*, 989−1001.
(25) Hillert, M.; Jansson, B. *J. Am. Ceram. Soc.* **1986**, *69*, 732−734.
(26) Ling, S. *Phys. Rev. B* **1994**, *49*, 864−880.
(27) Bulfin, B.; Murphy, B.; Lubben, O.; Krasnikov, S.; Shvets, I. *Int. J. Hydrogen Energy* **2012**, *37*, 10028−10035.
(28) Silbey, R. J.; Alberty, R. A.; Bawendi, M. G. *Physical Chemistry*, 4th ed.; Wiley: Hoboken, NJ, 2005.
(29) Panlener, R.; Blumenthal, R.; Garnier, J. *J. Phys. Chem. Solids* **1975**, *36*, 1213−1222.
(30) Dawicke, J. W.; Blumenthal, R. N. *J. Electrochemi. Soc.* **1986**, *133*, 904−909.
(31) Campserveux, J.; Gerdanian, P. *J. Solid State Chem.* **1978**, *23*, 73−92.
(32) Kitayama, K.; Nojiri, K.; Sugihara, T.; Katsura, T. *J. Solid State Chem.* **1985**, *56*, 1−11.
(33) Iwaski, B.; Katsura, T. *Bull. Chem. Soc. Jpn.* **1970**, *44*, 1297−1301.
(34) Kamiya, M.; Shimada, E.; Ikuma, Y.; Komatsu, M.; Haneda, H. *J. Electrochem. Soc.* **2000**, *147*, 1222−1227.
(35) Giordano, F.; Trovarelli, A.; de Leitenburg, C.; Dolcetti, G.; Giona, M. *Ind. Eng. Chem. Res.* **2001**, *40*, 4828−4835.
(36) VanHandel, G. J.; Blumenthal, R. N. *J. Electrochem. Soc.* **1974**, *121*, 1198−1202.
(37) Stan, M.; Zhu, Y. T.; Jiang, H.; Butt, D. P. *J. Appl. Phys.* **2004**, *95*, 3358−3361.
(38) Le Gal, A.; Abanades, S. *Int. J. Hydrogen Energy* **2011**, *36*, 4739−4748.

(39) Meng, Q.-L.; il Lee, C.; Shigeta, S.; Kaneko, H.; Tamaura, Y. *J. Solid State Chem.* **2012**, *194*, 343−351.
(40) Balducci, G.; Islam, M. S.; Kapar, J.; Fornasiero, P.; Graziani, M. *Chem. Mater.* **2000**, *12*, 677−681.
(41) Levenspiel, O. *Chemical Reaction Engineering*; John Wiley & Sons: New York, 1999.
(42) Paier, J.; Penschke, C.; Sauer, J. *Chem. Rev.* **2013**, *113*, 3949−3985.
(43) Ramos-Fernandez, E. V.; Shiju, N. R.; Steinfeld, A.; Rothenberg, G. Producing CO from CO_2 by Redox Cycling Using Doped Cerias. *Proceedings of 2nd International Conference on Materials for Energy, ENMAT II*, Karlsruhe, Germany, May 12−16, 2013.
(44) Meng, Q.-L.; il Lee, C.; Ishihara, T.; Kaneko, H.; Tamaura, Y. *Int. J. Hydrogen Energy* **2011**, *36*, 13435−13441.
(45) Kang, K.-S.; Kim, C.-H.; Park, C.-S.; Kim, J.-W. *J. Ind. Eng. Chem.* **2007**, *13*, 657−663.
(46) Andersson, D. A.; Simak, S. I.; Skorodumova, N. V.; Abrikosov, I.; Johansson, B. *Appl. Phys. Lett.* **2007**, *90*, 031909-1−031909-3.

dx.doi.org/10.1021/jp406578z | *J. Phys. Chem. C* XXXX, XXX, XXX−XXX